

# Fully stable numerical calculations for finite one-dimensional structures: mapping the Transfer Matrix method

Jose Miguel Luque-Raigon,<sup>1,2,\*</sup> Janne Halme,<sup>1</sup> and Hernan Miguez,<sup>2</sup>

<sup>1</sup>*Department of Applied Physics, Aalto University School of Science, P.O. Box 15100, FI-00076, AALTO, Finland*

<sup>2</sup>*Instituto de Ciencia de Materiales de Sevilla (CSIC), C/Américo Vespucio, 49, 41092 Sevilla, Spain*

\*[jose.luque.raigon@aalto.fi](mailto:jose.luque.raigon@aalto.fi)

## Abstract

We design a fully stable numerical solution of the Maxwell's equations with the Transfer Matrix Method (TMM) to understand the interaction between an electromagnetic field and a finite, one-dimensional, non-periodic structure. Such an exact solution can be tailored from a conventional solution by choosing an adequate transformation between its reference systems, which induces a mapping between its associated TMMs. The paper demonstrates theoretically the numerical stability of the TMM for the exact solution within the framework of Maxwell's equations, but the same formalism can efficiently be applied to resolve other classical or quantum linear wave-propagation interaction in one, two, and three dimensions. This is because the formalism is exclusively built up for an in depth analysis of the TMM's symmetries.

**PACS:** 78.20.Bh; 78.20.Ci; 42.25.Bs

**OCIS codes:** (000.3860) Mathematical methods in physics; (000.4430) Numerical approximation and analysis; (260.2110) Electromagnetic optics; (350.4238) Nanophotonics and photonic crystals.

## 1. Introduction

Understanding the interaction between radiation and matter at the nanoscale is fundamental for achieving optimal control of the radiation flux in nanostructures [1]. The analytical and numerical calculations are the tools used to design these nanostructures in specific scientific and technological applications. Nevertheless, efficient numerical calculations in complex, multiscale nanostructures require a balance between computer time and numerical accuracy because improving one could make the other worse. For this reason, it is important to develop new efficient and accurate analytical and/or numerical methods to resolve the interactions that take place within nanostructures. The simultaneous optimization of computational efficiency and accuracy makes it possible a detailed understanding of the multi-scale, internal behavior of some nanostructures, such as photonic crystals (PC), dye-sensitized solar cells (DSSC), and other complex optical structures, which can incorporate *a*) emitted nanostructures, such as atoms, quantum dots, or fluorescent molecules, and/or *b*) absorptive nanostructures, such as glasses, metals, carbon nanotubes, or polymeric components [2].

The transfer matrix method (TMM) is a simple, accurate, low-computer-time formalism that can be used for resolving wave equations because of its low matrix dimensionality. Nevertheless, the TMM calculations could show numerical instabilities (inaccuracies and/or singularities) in some specific multilayer conditions proposed in the literature [3-6]. These numerical instabilities can be resolved by using different formalisms. The TMM can be transformed into the Scattering Matrix Method (SMM), which makes it possible to avoid exponential numerical instabilities [6]. Other formalisms expand the TMM solution on a non-exponential basis, but this non-natural basis could introduce its own instabilities [7]. One TMM approach partially removes the exponential numerical instabilities [4], but they can still appear in some extreme conditions such as with highly absorbing layers and/or with high thickness/wavelength ratios. An interesting TMM formalism is the enhanced transmittance matrix approach, which resolves the exponential instabilities for the total transmittance, reflectance, and absorptance of the multilayer by introducing some scales [5]. One study has considered the invariant scaling symmetry of Maxwell's equations to obtain a TMM that avoids the exponential instabilities, but

these expressions are complicated both analytically and numerically [3], because they do not take into account the particular natural symmetries of the TMM.

The objective of the present study is to design a formalism to achieve an exact solution of the Maxwell's equations in the TMM representation, in the sense of an analytical solution that is fully stable for numerical calculations in any kind of multilayer structure. We demonstrate such an exact solution by developing a geometrical formalism—the symmetry-based method (SBM)—which corrects, extends, and unifies the rest of formalisms provided in other studies [3-5, 7]. We intend here extend and generalize the ideas proposed in reference [5], by finding the symmetries subjacent to the TMM that can be applied in the control not only of the scales (real exponential components), as proposes in reference [5], but even of the phases (imaginary exponential components). The symmetry properties of the TMM are the only considerations employed in the SBM to reach this analytical solution, which entails applying general conclusions from the present work not only to Maxwell's equations but also to any linear classical or quantum system where oscillations or wave propagations (for example, acoustic, electromagnetic, electronic or spin) are considered [8-12].

The SBM allows to obtain the exact solution of the Maxwell's equations from one conventional solution as a mapping between its TMMs induced from the transformation in the solution's associated reference systems. These mappings are made up and parameterized in the TMM using its external symmetries – that is, geometrical objects that commute with all the geometrical constituent objects of the TMM – that have a structure of 2-degenerate, diagonal, two-dimensional matrices with parameterized exponential components. These external symmetries allow building up a natural basis of the TMM. The exact solution of the Maxwell's equations can then be chosen from the parameterized set of mappings by imposing to the parameters the condition that the accumulation of both exponential and non-exponential numerical instabilities are fully compensated and resolved.

## 2. The conventional solution in the transfer matrix method representation

We consider a classical interaction between the electromagnetic radiation and a finite, one-dimensional, non-periodic multilayer, where the corresponding Maxwell's equations are solved in the TMM formalism. This interaction system fulfills the same conditions proposed by Yeh [4]. The propagation of the electromagnetic fields are represented by forward (noted with super-index +) and backward (noted with super-index -) waves, in both  $s$ -polarization and  $p$ -polarization modes, and for each homogeneous-isotropic  $j$ -region of the multilayer (layers and external media), where  $j = 0, n + 1$  stand for external media and  $j = 1, \dots, n$  for the layers. The different layers and the external media are called as regions and there are interfaces between consecutive regions. The wave propagation for frequency  $\omega$  is provided by the electric field solution  $\tilde{\mathbf{E}}(\mathbf{r}, t) = \tilde{\mathbf{E}}(\mathbf{r})e^{i\omega t}$  (see Fig. 1), where the spatial electric field part is given by the following equation:

$$\tilde{\mathbf{E}}(\mathbf{r}) = \begin{cases} (1 \ 1)(\mathbf{P}_0^{-1})_{y-y_0} \begin{pmatrix} 1 \\ \tilde{E}_0^- \end{pmatrix} e^{-i\tilde{\alpha}x} & \text{with } y \in (-\infty, y_0); \ x \in (x_0, +\infty) \\ (1 \ 1)(\mathbf{P}_j^{-1})_{y-y_{j-1}} \begin{pmatrix} \tilde{E}_j^+ \\ \tilde{E}_j^- \end{pmatrix} e^{-i\tilde{\alpha}x} & \text{with } y \in (y_{j-1}, y_j); \ x \in (x_0, +\infty) \end{cases} \quad (1)$$

where  $j = 1, \dots, n, n + 1$ , for the forward and backward electric field amplitudes  $\tilde{E}_j^+, \tilde{E}_j^-$ . The boundary conditions impose that there is not backward wave in the outgoing medium  $\tilde{E}_{n+1}^- = 0$ , and forward wave in the incoming medium is normalized to one  $\tilde{E}_0^+ = 1$ . Additionally, external media are bounded by positions  $y_{-1} = -\infty, y_{n+1} = +\infty$ . The complex wavevector at each region is defined by  $\tilde{\mathbf{k}}_j = (2\pi\tilde{n}_j(\lambda)/\lambda)[\cos(\tilde{\theta}_j)\hat{\mathbf{y}} + \sin(\tilde{\theta}_j)\hat{\mathbf{x}}] = \tilde{\beta}_j\hat{\mathbf{y}} + \tilde{\alpha}_j\hat{\mathbf{x}}$  for the wavelength  $\lambda$  at the complex angle  $\tilde{\theta}_j$

and complex refractive index  $\tilde{n}_j(\lambda)$  (see Fig. 1). The complex wavevector projections  $\tilde{\beta}_j, \tilde{\alpha}$  fulfill the conditions  $Im(\tilde{\beta}_j) \leq 0$  and  $Im(\tilde{\alpha}) \leq 0$ . The partial propagation matrices introduced in (1) are given by

$$(\mathbf{P}_0)_{y-y_0} \equiv \begin{pmatrix} e^{i\tilde{\beta}_0(y-y_0)} & 0 \\ 0 & e^{-i\tilde{\beta}_0(y-y_0)} \end{pmatrix}; \quad (\mathbf{P}_j)_{(y-y_{j-1})} \equiv \begin{pmatrix} e^{i\tilde{\beta}_j(y-y_{j-1})} & 0 \\ 0 & e^{-i\tilde{\beta}_j(y-y_{j-1})} \end{pmatrix} \quad (2)$$

where  $(\mathbf{P}_j)_{(y-y_{j-1})}$  describes the electromagnetic behaviour in the  $y$ -point of the  $j$ -region with respect to that region's own origin situated at the interface point  $y_{j-1}$ . Note that  $(\mathbf{P}_0)_{y-y_0}$  has an equivalent interpretation for the incoming external medium. The TMM provides the propagation of the electric field amplitudes through the multilayer structure, and it can be obtained using the following relations:

$$\begin{pmatrix} \tilde{E}_j^+ \\ \tilde{E}_j^- \end{pmatrix} = \mathbf{D}_j^{-1} [\mathbf{D}_{j-1} \mathbf{P}_{j-1}^{-1} \mathbf{D}_{j-1}^{-1}] [\mathbf{D}_{j-2} \mathbf{P}_{j-2}^{-1} \mathbf{D}_{j-2}^{-1}] \cdots [\mathbf{D}_1 \mathbf{P}_1^{-1} \mathbf{D}_1^{-1}] \mathbf{D}_0 \begin{pmatrix} 1 \\ \tilde{E}_0^- \end{pmatrix} \quad \text{with } j = 1, \dots, n+1$$

$$\text{where } \mathbf{P}_j = \begin{pmatrix} e^{i\tilde{\beta}_j(y_j-y_{j-1})} & 0 \\ 0 & e^{-i\tilde{\beta}_j(y_j-y_{j-1})} \end{pmatrix}; \quad \mathbf{D}_j = \begin{cases} \begin{pmatrix} 1 & 1 \\ \tilde{n}_j \cos(\tilde{\theta}_j) & -\tilde{n}_j \cos(\tilde{\theta}_j) \end{pmatrix} & s\text{-polarization} \\ \begin{pmatrix} \cos(\tilde{\theta}_j) & \cos(\tilde{\theta}_j) \\ \tilde{n}_j & -\tilde{n}_j \end{pmatrix} & p\text{-polarization} \end{cases} \quad (3)$$

where  $\mathbf{D}_j$  and  $\mathbf{D}_{j-1}$  are the dynamic matrices describing the boundary condition at the interface between the regions  $j-1$  and  $j$ , and  $\mathbf{P}_j$  is the propagation matrix describing the propagation along the whole region  $j$ . Note that the forward and backward field amplitudes  $\tilde{E}_j^+$  and  $\tilde{E}_j^-$  are defined at the beginning of the  $j$ -layer when considering the direction of the increasing indices (that is, the TMM propagation direction); this is apparent from the physical sense of the defined matrices. The equation set (1), (2) and (3) is the conventional solution for the interaction system in the TMM representation [4], but expressed in

a new formalism using partial propagation matrices defined in equation (2). The expressions of (1) and (3) can be combined to give an expression that depends only on the dynamic, propagation and partial propagation matrices:

$$\tilde{\mathbf{E}}(\mathbf{r}) = \begin{cases} (1 \quad 1)(\mathbf{P}_0^{-1})_{y-y_0} \begin{pmatrix} 1 \\ \tilde{\mathbf{E}}_0^- \end{pmatrix} e^{-i\tilde{\alpha}x} & \text{with } y \in (-\infty, y_0); \quad x \in (x_0, +\infty) \\ (1 \quad 1)(\mathbf{P}_j^{-1})_{(y-y_{j-1})} \mathbf{D}_j^{-1} [\mathbf{D}_{j-1} \mathbf{P}_{j-1}^{-1} \mathbf{D}_{j-1}^{-1}] [\mathbf{D}_{j-2} \mathbf{P}_{j-2}^{-1} \mathbf{D}_{j-2}^{-1}] \dots [\mathbf{D}_1 \mathbf{P}_1^{-1} \mathbf{D}_1^{-1}] \mathbf{D}_0 \begin{pmatrix} 1 \\ \tilde{\mathbf{E}}_0^- \end{pmatrix} e^{-i\tilde{\alpha}x} & \text{with } y \in (y_{j-1}, y_j); \quad x \in (x_0, +\infty) \end{cases} \quad (4)$$

with  $j = 1, \dots, n+1$ . The conventional solution in the TMM representation provided in Eq. (4) resolves the exponential numerical instabilities in more typical interaction conditions, but fails to do so in some extreme conditions, such as those involving highly absorbing layers and/or high thickness/wavelength ratios. In the next section, we develop and apply a symmetry based method (SBM) to obtain from the conventional solution of Eq. (4) an exact solution that fully avoids both exponential and non-exponential numerical instabilities of the TMM.

### 3. The exact solution in the transfer matrix method representation

The TMM shows both exponential numerical instabilities which arise from the inversion of both the propagation matrices  $\mathbf{P}_j$  and the partial propagation matrices  $(\mathbf{P}_j)_{(y-y_{j-1})}$ , and non-exponential numerical instabilities arising from the inversion of the dynamic matrices  $\mathbf{D}_j$ .

The exponential numerical instabilities come from systems where the inversion of any partial propagation matrices (or inverted propagation matrices) provides a numerically singular TMM. The singular inverted matrix conditions for the  $j$ -region are found in the extreme conditions

$\text{Im}(\tilde{\beta}_j) \ll 0$  and  $y - y_{j-1} \gg 0$ . In this case, the partial propagation matrix of the  $j$ -region manifests an asymptotic behavior,

$$(\mathbf{P}_j)_{(y-y_{j-1})}^{-1} \xrightarrow[\substack{\text{Im}(\tilde{\beta}_j) \ll 0 \\ y_j - y_{j-1} \gg 0}]{} \begin{pmatrix} e^{-|\text{Im}(\tilde{\beta}_j)|(y-y_{j-1})} & 0 \\ 0 & e^{+|\text{Im}(\tilde{\beta}_j)|(y-y_{j-1})} \end{pmatrix} \quad (5)$$

which *mutatis mutandis* is the same for the  $j$ -region propagation matrix. The asymptotic form in Eq. (5) is averaged in the oscillatory components, thereby fulfilling the criteria that  $|\text{Im}(\tilde{\beta}_j)|(y - y_{j-1}) \geq 0$  is a real number. If the value of this real number is sufficiently high, then the decreasing exponential component could approach numerically zero, producing a numerically singular matrix (instability) that accumulates and propagates in the recursive matrix multiplications of TMM. The solution of these instabilities requires a matrix factorization that follows the asymptotic behavior:

$$(\mathbf{P}_j)_{(y-y_{j-1})}^{-1} \xrightarrow[\substack{\text{Im}(\tilde{\beta}_j) \ll 0 \\ y_j - y_{j-1} \gg 0}]{} \begin{pmatrix} e^{-|\text{Im}(\tilde{\beta}_j)|(y-y_{j-1})} & 0 \\ 0 & e^{-|\text{Im}(\tilde{\beta}_j)|(y-y_{j-1})} \end{pmatrix} \begin{pmatrix} 1 & 0 \\ 0 & e^{+2|\text{Im}(\tilde{\beta}_j)|(y-y_{j-1})} \end{pmatrix} \quad (6)$$

where the first matrix is not involved in the TMM calculations because as a matrix of symmetry it can be extracted from the TMM structure. This leaves in the TMM calculations only the second matrix that is a regular numerical matrix (numerically non-singular). The matrix factorization thus resolves the exponential instability problem and is the central keystone in the SBM.

In addition to the exponential instabilities resolved by the matrix factorization (6), there can be also non-exponential numerical instabilities. These come from systems where the inverted dynamic matrices

show numerical instabilities due to very low values of the terms  $\left[-2\tilde{n}_j \cos(\tilde{\theta}_j)\right]^{-1} < 1$ . Such a situation could appear in a multilayer that has a huge number of interfaces, through accumulation of the values of the above mentioned terms, and/or from interfaces with high absolute values of the complex refractive index. In the following, we show that simultaneous solution of both exponential and non-exponential instabilities can be achieved in a unified manner by introducing the external symmetries of the TMM.

Our aim is to identify the external symmetries associated with the conventional solution Eq. (4). This equation (4) is original in the sense that it shows the solution of the Maxwell's equations expressed exclusively in terms of dynamic, propagation and partial propagation matrices. Therefore, the recursive rules generating the TMM propagation (not be confused with the wave propagations) are given as a matrix function that depends on the spatial point  $y$ . As a consequence, the TMM propagation by matrix multiplications in equation (4) is described point-by-point. This fact allows a point-by-point handling of the TMM structure via its external symmetries, which can be used to control the numerical instabilities coming from the point-by-point numerical accumulations through the dynamic, propagation and partial propagation matrices.

For controlling the instabilities, we use in the SBM tailored external symmetries to act point-by-point upon the dynamic, partial propagation and propagation matrices to modify the numerical behavior of the conventional TMM while preserving its structure. Mathematically, this requires that the external symmetries must commute with the entire point-dependent matrices constituting the TMM structure. Because of this requirement, we call the *external symmetries* as opposed to the *internal symmetries* that can commute in (3) only within each region separately. The  $2 \times 2$  dynamic and propagation matrices that are components of the TMM structure do not commute between themselves; therefore, in general it is not possible to extract them from the TMM structure without changing this structure. This means that the dynamic and propagation matrices are not external symmetries of the TMM representation. However, any degenerate, diagonal, 2-matrix, that is a two-dimensional matrix with only one 2-degenerate eigenvalue, commutes in a point-by-point manner with the dynamic, propagation and partial propagation



matrices of the TMM; and therefore, can be used as external symmetries of the conventional solution in the TMM representation given in Eq. (4). The main component in these 2-degenerate diagonal matrices is an arbitrary complex number that is introduced with a parameter that needs to be assigned a suitable value to control and avoid the numerical stability.

The exponential numerical instabilities come from an accumulation in the propagation matrices; therefore, a degenerate, diagonal, 2-matrix with exponential components can undo this accumulation in a natural manner. For this reason, the parameterized external symmetries for the entire  $j$ -region,  $\mathbf{A}_j^\pm(\varphi_j, \nu_j)$ , with  $j = 1, \dots, n+1$  and parameterization in the real phase-scale  $(\varphi_j, \nu_j)$ , are introduced as

$$\mathbf{A}_j^\pm(\varphi_j, \nu_j) \equiv \begin{pmatrix} e^{\mp(i\varphi_j + \nu_j)} & 0 \\ 0 & e^{\mp(i\varphi_j + \nu_j)} \end{pmatrix} \quad (7)$$

where  $\mathbf{A}_0^\pm(\varphi_0, \nu_0) \equiv \mathbf{I}$  is defined as the identity matrix, corresponding to a phase-scale  $\varphi_0 = \nu_0 = 0$ . We introduce the inverse parameterized symmetries of Eq. (7) through the relations  $\mathbf{A}_j^\pm(\varphi_j, \nu_j)\mathbf{A}_j^\pm(\varphi_j, \nu_j)^{-1} = \mathbf{A}_j^\pm(\varphi_j, \nu_j)\mathbf{A}_j^\mp(\varphi_j, \nu_j) = \mathbf{I}$ , with  $j = 1, \dots, n+1$ . Note that the set of parameterized external symmetries derived from Eq. (7) constitute an abelian Lie group parameterized in the continuous parameter phase-scale  $(\varphi_j, \nu_j)$ .

The external symmetries of Eq. (7) are the adequate operators to act on the dynamic, propagation and partial propagation matrices in order to avoid an accumulation of instabilities, thereby preserving their position in the TMM structure. Therefore, these external symmetries can be used to expand the conventional solution in the exact solution, which is the key advantage of the SBM. The conventional solution derived from Eq. (4) is modified through the action of the symmetries in Eq. (7) in the parameterized form given by

$$\tilde{\mathbf{E}}(\mathbf{r}') = \begin{cases} (1 \ 1) (\mathbf{P}_0^{-1})_{y-y_0} \begin{pmatrix} 1 \\ \tilde{E}_0^- \end{pmatrix} e^{-i\tilde{\alpha}x} & \text{with } y \in (-\infty, y_0); \quad x \in (x_0, +\infty) \\ (1 \ 1) [(\mathbf{P}_j^{-1})_{y'_f, y'_b} \mathbf{D}_j^{-1}] [\mathbf{D}_{j-1} \mathbf{A}_{j-1}^\pm (\varphi_{j-1}, \nu_{j-1})^{-1} \mathbf{P}_{j-1}^{-1} \mathbf{D}_{j-1}^{-1}] \cdot \\ \cdot [\mathbf{D}_{j-2} \mathbf{A}_{j-2}^\pm (\varphi_{j-2}, \nu_{j-2})^{-1} \mathbf{P}_{j-2}^{-1} \mathbf{D}_{j-2}^{-1}] \cdot \dots \cdot [\mathbf{D}_1 \mathbf{A}_1^\pm (\varphi_1, \nu_1)^{-1} \mathbf{P}_1^{-1} \mathbf{D}_1^{-1}] \mathbf{D}_0 \begin{pmatrix} 1 \\ \tilde{E}_0^- \end{pmatrix} e^{-i\tilde{\alpha}x} & \\ \text{with } y \in (y_{j-1}, y_j); \quad x \in (x_0, +\infty) & \end{cases} \quad (8)$$

with  $j=1, \dots, n+1$ . The new matrices,  $(\mathbf{P}_j^{-1})_{y'_f, y'_b}$ , are defined below in Eq. (9) and explained its physical sense in the subsequent text. The expression in Eq. (8) shows how the position invariant propagation matrices,  $\mathbf{P}_{j-1}$ , are operated by the parameterized external symmetries,  $\mathbf{A}_{j-1}^\pm(\varphi_{j-1}, \nu_{j-1})$ , which represent a parameterized transformation through the parameters  $(\varphi_{j-1}, \nu_{j-1})$  and correspond to a translation-phase and dilatation-scale, respectively. Therefore, the expression in Eq. (8) defines a new parameterized TMM in the reference system,  $\mathbf{r}' = (\mathbf{y}', \mathbf{x})$ , one which preserves its structure only when the invariant relationships are fulfilled:

$$\tilde{\mathbf{E}}(\mathbf{r}) = \tilde{\mathbf{E}}(\mathbf{r}') \Leftrightarrow (\mathbf{P}_j^{-1})_{(y-y_{j-1})} \begin{pmatrix} \tilde{E}_j^+ \\ \tilde{E}_j^- \end{pmatrix} = \mathbf{M}_{j-1}^\pm(\varphi_1, \nu_1, \dots, \varphi_{j-1}, \nu_{j-1}) (\mathbf{P}_j^{-1})_{y'_f, y'_b} \begin{pmatrix} \tilde{E}_j^+ \\ \tilde{E}_j^- \end{pmatrix};$$

$$\text{where } \mathbf{M}_{j-1}^\pm(\varphi_1, \nu_1, \dots, \varphi_{j-1}, \nu_{j-1}) \equiv \mathbf{A}_1^\pm(\varphi_1, \nu_1) \cdot \dots \cdot \mathbf{A}_{j-2}^\pm(\varphi_{j-2}, \nu_{j-2}) \mathbf{A}_{j-1}^\pm(\varphi_{j-1}, \nu_{j-1}); \quad (9)$$

$$\text{and } (\mathbf{P}_j^{-1})_{(y-y_{j-1})} \equiv \begin{pmatrix} e^{-i\tilde{\beta}_j(y-y_{j-1})} & 0 \\ 0 & e^{+i\tilde{\beta}_j(y-y_{j-1})} \end{pmatrix}; \quad (\mathbf{P}_j^{-1})_{y'_f, y'_b} \equiv \begin{pmatrix} e^{-i\tilde{\beta}_j y'_f} & 0 \\ 0 & e^{+i\tilde{\beta}_j y'_b} \end{pmatrix}$$

for all  $j=1, \dots, n+1$ . The matrices,  $(\mathbf{P}_j^{-1})_{y'_f, y'_b}$ , are introduced for the phase-scale decoupling between the forward and backward waves in the reference system,  $\mathbf{r}' = (\mathbf{y}', \mathbf{x})$ . Therefore, the invariant relations

in Eq. (9) represent a parameterized point-by-point mapping between the conventional TMM derived from equation (4) and any other parameterized TMM where the parameter fixes the TMM. This mapping is associated with a parameterized reference system transformation that is split into forward and backward waves as follows:

$$(y - y_{j-1}) \rightarrow \begin{cases} y'_f = (y - y_{j-1}) \mp \sum_{k=1}^{j-1} (i\varphi_k + \nu_k) / i\tilde{\beta}_j & \text{for forward wave} \\ y'_b = (y - y_{j-1}) \pm \sum_{k=1}^{j-1} (i\varphi_k + \nu_k) / i\tilde{\beta}_j & \text{for backward wave} \end{cases} \quad (10)$$

where  $j = 1, \dots, n+1$ . The parameterized reference system transformation  $\mathbf{r} = (\mathbf{y}, \mathbf{x}) \rightarrow \mathbf{r}' = (\mathbf{y}', \mathbf{x})$  given in (10) maps the conventional solution (4) into a new parameterized solution and at the same time the associated TMMs. Therefore, it is possible to undo the accumulation in the TMM propagation in an exact manner if we choose an adequate parameter,  $i\varphi_k + \nu_k$ . The mapping defined in Eq. (9) represents an expansion of the conventional solution from Eq. (8) in a new, parameterized, arbitrary solution. This expansion generates a set of discrete parameterized  $j-1$  components,  $\mathbf{M}_{j-1}^\pm$ , which are built up with the external symmetries of the TMM, and are defined as follows:

$$\begin{aligned} \mathbf{M}_0^\pm &= \mathbf{I}; \\ \mathbf{M}_1^\pm &= \mathbf{A}_1^\pm(\varphi_1, \nu_1); \\ \mathbf{M}_2^\pm &= \mathbf{A}_1^\pm(\varphi_1, \nu_1)\mathbf{A}_2^\pm(\varphi_2, \nu_2); \\ &\vdots \\ \mathbf{M}_{j-1}^\pm &= \mathbf{A}_1^\pm(\varphi_1, \nu_1)\mathbf{A}_2^\pm(\varphi_2, \nu_2) \cdots \mathbf{A}_{j-2}^\pm(\varphi_{j-2}, \nu_{j-2})\mathbf{A}_{j-1}^\pm(\varphi_{j-1}, \nu_{j-1}). \end{aligned} \quad (11)$$

where  $j = 1, \dots, n+1$ . The components in Eq. (11) represent the matrix correction of the discrete region-by-region accumulation coming from the TMM propagation. Note that the up-signs (+) of

$\mathbf{A}_{j-1}^{\pm}(\varphi_{j-1}, \nu_{j-1})$  represent the correction when the TMM is propagating in the forward wave direction, while the corresponding down-sign ( $-$ ) is for the correction when the TMM is propagating in the backward wave direction.

The parameterized solution derived from Eqs. (8), (9), (10), and (11) needs to be evaluated by choosing the up or down sign (which indicates the TMM propagation direction) and the parameters (which need be tailored to resolve the exponential instabilities of the TMM). We must consider the up-sign in this solution because the TMM propagation was defined in the same direction as the forward wave (the direction in which the numerical instability accumulates). We know that the phase-scale accumulation in the TMM, that is propagated in the forward wave direction and localized in the  $j$ -layer position, has the components  $i\varphi_k + \nu_k = i\tilde{\beta}_k d_k$ , where the crossed layers are given by  $k = 1, \dots, j-1$ .

Consequently, the total phase-scale accumulation is given by the sum  $\sum_{k=1}^{j-1} i\tilde{\beta}_k d_k$ . The reference system transformation, which corrects this accumulation in an exact manner, is given for the parameters  $i\varphi_k + \nu_k = i\tilde{\beta}_k d_k$ , where  $k = 1, \dots, j-1$ . Therefore, the reference system transformation between the conventional and exact solutions is given by

$$(y - y_{j-1}) \rightarrow \begin{cases} y'_f = (y - y_{j-1}) - \sum_{k=1}^{j-1} (\tilde{\beta}_k / \tilde{\beta}_j) d_k & \text{for forward wave} \\ y'_b = (y - y_{j-1}) + \sum_{k=1}^{j-1} (\tilde{\beta}_k / \tilde{\beta}_j) d_k & \text{for backward wave} \end{cases} \quad (12)$$

with  $j = 1, \dots, n+1$ . Furthermore, the conventional solution (or its associated TMM) is expanded in the exact solution (or its associated TMM) by means of the accumulated external symmetries from Eq. (11), which are given by

$$\mathbf{M}_0^+ = \begin{pmatrix} 1 & 0 \\ 0 & 1 \end{pmatrix}, \quad \mathbf{M}_1^+ = \begin{pmatrix} e^{-i\sum_{k=1}^1 \tilde{\beta}_k d_k} & 0 \\ 0 & e^{-i\sum_{k=1}^1 \tilde{\beta}_k d_k} \end{pmatrix}, \dots, \quad \mathbf{M}_{j-1}^+ = \begin{pmatrix} e^{-i\sum_{k=1}^{j-1} \tilde{\beta}_k d_k} & 0 \\ 0 & e^{-i\sum_{k=1}^{j-1} \tilde{\beta}_k d_k} \end{pmatrix} \quad (13)$$

with  $j = 1, \dots, n+1$ . The reference system transformation in Eq. (12) corresponds to the expansion of the conventional solution to the exact solution through the matrix coefficients in Eq. (13). The exact solution is expressed in the reference system,  $\mathbf{r} = (\mathbf{y}, \mathbf{x})$ , as follows:

$$\tilde{\mathbf{E}}'(\mathbf{r}) = \begin{cases} (1 \quad 1) (\mathbf{P}_0^{-1})_{y-y_0} \begin{pmatrix} 1 \\ \tilde{E}_0^- \end{pmatrix} e^{-i\tilde{\alpha}x} & \text{with } y \in (-\infty, y_0); \quad x \in (x_0, +\infty) \\ (1 \quad 1) \begin{pmatrix} 1 & 0 \\ 0 & e^{i\sum_{k=1}^{j-1} \tilde{\beta}_k d_k + i\tilde{\beta}_j (y-y_{j-1})} \end{pmatrix} \begin{pmatrix} \tilde{E}_j^+ \\ \tilde{E}_j^- \end{pmatrix} e^{-i\tilde{\alpha}x} & \text{with } y \in (y_{j-1}, y_j); \quad x \in (x_0, +\infty) \end{cases} \quad (14)$$

where  $j = 1, \dots, n+1$ . The invariant relations (mapping), which link the electrical field amplitudes in both reference systems,  $\mathbf{r} = (\mathbf{y}, \mathbf{x})$  and  $\mathbf{r}' = (\mathbf{y}', \mathbf{x})$ , are expressed in the reference system,  $\mathbf{r} = (\mathbf{y}, \mathbf{x})$ , as follows:

$$\tilde{\mathbf{E}}_j(\mathbf{r}) = \mathbf{M}_{j-1}^+ \tilde{\mathbf{E}}'_j(\mathbf{r}) \quad \text{with } y \in (y_{j-1}, y_j); \quad x \in (x_0, +\infty) \quad \text{where} \quad (15)$$

$$\tilde{\mathbf{E}}_j(\mathbf{r}) = \begin{pmatrix} e^{-i\tilde{\beta}_j (y-y_{j-1})} & 0 \\ 0 & e^{+i\tilde{\beta}_j (y-y_{j-1})} \end{pmatrix} \begin{pmatrix} \tilde{E}_j^+ \\ \tilde{E}_j^- \end{pmatrix} e^{-i\tilde{\alpha}x}; \quad \tilde{\mathbf{E}}'_j(\mathbf{r}) = \begin{pmatrix} 1 & 0 \\ 0 & e^{i\sum_{k=1}^{j-1} \tilde{\beta}_k d_k + i\tilde{\beta}_j (y-y_{j-1})} \end{pmatrix} \begin{pmatrix} \tilde{E}_j^+ \\ \tilde{E}_j^- \end{pmatrix} e^{-i\tilde{\alpha}x}$$

where  $j = 1, \dots, n+1$ ;  $\tilde{E}_{n+1}^- = 0$  means there is no reflected waves in the outgoing medium, and  $\tilde{E}_0^+ = 1$  means the incident wave is normalized. The wavevector  $\tilde{\mathbf{k}}_j = (2\pi\tilde{n}_j(\lambda)/\lambda)[\cos(\tilde{\theta}_j)\hat{\mathbf{y}} + \sin(\tilde{\theta}_j)\hat{\mathbf{x}}]$   $= \tilde{\beta}_j\hat{\mathbf{y}} + \tilde{\alpha}_j\hat{\mathbf{x}}$  fulfills the conditions for non-emissive media,  $Im(\tilde{\beta}_j) \leq 0$ ,  $Im(\tilde{\alpha}_j) \leq 0$ . The coordinate origin for the exact solution is fixed by the boundary condition,  $y'_f = 0$ , represented in the  $\mathbf{r}' = (\mathbf{y}', \mathbf{x})$  reference system, which has an equivalent representation in the  $\mathbf{r} = (\mathbf{y}, \mathbf{x})$  reference system as follows

$$\begin{aligned} y'_f \Big|_{y=y_{0j}} &= (y - y_{j-1}) - \sum_{k=1}^{j-1} (\tilde{\beta}_k / \tilde{\beta}_j) d_k \Big|_{y=y_{0j}} = 0 \quad \text{with } y_{0j} \in j\text{-layer} \Rightarrow \\ \Rightarrow y_{0j} &= y_{j-1} + \sum_{k=1}^{j-1} (\tilde{\beta}_k / \tilde{\beta}_j) d_k \quad \text{origin for } j\text{-layer} \end{aligned} \quad (16)$$

with  $j = 1, \dots, n+1$ . That is means, if the coordinate origin of the exact solution in the reference system  $\mathbf{r}' = (\mathbf{y}', \mathbf{x})$  is fixed as  $y'_f = 0$ , then the exact solution has a set of origins by regions in the reference system  $\mathbf{r} = (\mathbf{y}, \mathbf{x})$  that are given by  $y_{0j}$ . Consequently, the exact solution in the reference system  $\mathbf{r} = (\mathbf{y}, \mathbf{x})$  is a region-by-region solution.

Eqs. (2), (3), (13), (14), and (15) provide the complete exact solution of the Maxwell's equations in the TMM representation which avoids point-by-point the exponential numerical instabilities that accumulate from the propagation of the TMM. This exact solution for the phase-scale parameter,  $i\varphi_k + \nu_k = i\tilde{\beta}_k d_k$ , represents an exact correction that is tailored to follow the dilation-oscillation changes in the propagation and partial propagation matrices of the TMM. Nevertheless, some extreme conditions in the multilayer structure, as it was said before, can generate non-exponential instabilities from the dynamic matrices. This can be handled by a new phase-scale parameter defined as

$$i\varphi_j + \nu_j \equiv im\tilde{\beta}_j d_j; \quad \text{where } j=1,2, \dots, n+1 \quad \text{and } m = 0,1,2,\dots \quad (17)$$

where the  $m \geq 1$  real parameter denotes the total correction with a component for the exponential  $m_E = 1$  and non-exponential  $m_{NE} = m - m_E$  instabilities. From an application point of view, the new exact solution can be obtained by substituting  $i\tilde{\beta}_k d_k \rightarrow im\tilde{\beta}_k d_k$  in Eqs. (13), (14), and (15). Note that the reference system transformation in Eq. (16) is the same for all  $m \geq 1$ , which means that this parameter takes into account additional corrections  $m_{NE}$  of phase-scale that come exclusively from the dynamic matrices because they have invariant position in the TMM structure. The development of the procedure for obtaining the  $m$ -parameter provides a tunable exact solution where the total phase-scale of the instability problem can be handled with one and same parameter  $m$ . Nevertheless, the independent layers, phases, and scales can be considered through the dependence  $m \equiv m_j(\varphi_j, \nu_j)$ , that is,  $m$  can independently take a different value in each  $j$ -layer, which is evident and compatible with the Eqs. (13), (14), and (15).

#### 4. Calculations and results

In the previous theoretical section, we analytically demonstrated for Maxwell's equations how to obtain an exact solution from a conventional solution in the TMM representation by using the SBM. In this section, we present numerical calculations for both solutions to show their numerical behavior. The numerical calculations were performed using Matlab version 7.11.0.584 (R2010b) software and an Intel Xeon CPU E3-1230 @ 3.20 GHz processor.

The validation of the exact solution (section 3) is illustrated for a dye-sensitized solar cell (DSSC) by comparing the calculations from present work with the calculations (based on the conventional TMM) as well as experimental data from reference [13]. To facilitate the comparison we have applied a moving average broadband-window filter to our calculations. This filter models the smoothing effect (optical

incoherency) that arises mainly from the limited spectral band-width of optical measurement instruments and is always present to some extent in experimental optical data, including reference [13]. The Fig. 2 shows the total reflectance (1a), total transmittance (1b) and total absorptance (1c) for that DSSC working at normal incident angle (angle 0) having a porous  $\text{TiO}_2$  photoelectrode with thickness  $8.3 \mu\text{m}$  and sensitized with dye Z907. The detailed DSSC structure and optical parameters, i.e. thicknesses and complex refractive indices for layers, are taken from the reference [13]. The correlation between our simulation and the simulation and measured data from reference [13] is good as can be seen in Fig. 2, where the accuracy is better than 4% for the wavelength range 400-1400 nm, which validates our exact solution with respect to both the model and the experiments in reference [13].

Additionally, we have compared in this DSSC calculation the time consumption for both solutions: the conventional solution (section 2 of present paper) and our exact solution (section 3 of present paper). The time consumption for calculating all the simulated information shown in Fig. 2 (i.e reflectance, transmittance and absorptance in the wavelength range 400-1400 nm and wavelength resolution 1 nm) are the same for both algorithms (approx. 3.2-3.3 seconds), which means that the exact solution does not provide any advantage in terms of consumption of computational resources. This is evident from the fact that the ill- and well-conditioned models have essentially same numerical structure and therefore consume approximately equally amount of computer time. The purpose of the well-conditioned model was not to improve computational speed, but to improve the numerical stability. The case represented in Figure 2 serves here merely the purpose of model validation and verification, but was not critical with respect to numerical stability: the data in Figure 2 could be successfully and accurately obtained both with the ill- and well-conditioned models.

To demonstrate the improved numerical stability, we consider the modified DSSC structure presented in Figure 1. The thick and highly absorbing metallic titanium layer that acts as the counter electrode substrate in this DSSC configuration is much more challenging for the numerical optical calculations, for the reasons discussed in the theoretical sections. As an example, we consider how the incoming radiation



is absorbed by the different layers in the device structure at wavelength range between 400 and 800 nm and at incident angles 0, 40 and 80 degrees. The incoming and outgoing external media are constituted by air, and the layers are given by a thick glass ( $\tilde{n}_1, d_1 = 3.88 \text{ mm}$ ), an FTO, fluorine-doped tin oxide ( $\tilde{n}_2, d_2 = 697 \text{ nm}$ ), a dyed-photoelectrode, N719-electrolyte- $\text{TiO}_2$  ( $\tilde{n}_3, d_3 = 14 \mu\text{m}$ ), a tri-iodine electrolyte ( $\tilde{n}_4, d_4 = 11 \mu\text{m}$ ), a thin platinum layer ( $\tilde{n}_5, d_5 = 20 \text{ nm}$ ), and a titanium layer ( $\tilde{n}_6, d_6 = 30 \mu\text{m}$ ) (see Fig. 1). The complex refractive indices for these stacks are shown in Fig. 3 where it is possible to see the high differences in the magnitude order ( $\approx 10^5$ ) associated with the imaginary part of the refractive index. The refractive indices of metals were taken from reference [14], while the refractive indices of dielectrics were taken from reference [13].

Fig. 4 shows the exact solution calculations ( $m = 1$ ) at angles 0, 40 and 80 degrees for the total reflectance, total transmittance, and light absorptance by the different layers at each wavelength. The calculation using the conventional solution ( $m = 0$ ) is not represented since the solution is completely unstable. Therefore, Fig. 4 demonstrates that the proposed theoretical development works in a stable manner for the wavelength range 400-800 nm and at incident angles 0-80 degrees, where  $s$ -polarization and  $p$ -polarization modes have been averaged to represent un-polarized light. The wavelength range was selected according to the typical operation of a DSSC.

The Fig. 4 was achieved from the electric field amplitudes by layers calculated from our SBM; these amplitudes were introduced in the Poynting Theorem in order to achieve the normalized spectral photon flux density  $\phi_\lambda(y)$  as depending on the multilayer position  $y$ . The calculation providing the spectral absorption in each  $j$ -layer (Fig. 4) is the following  $A_j(\lambda) = A_{y_{j-1} < y < y_j}(\lambda) = \phi_\lambda(y_{j-1}) - \phi_\lambda(y_j)$ , where  $j$ -layer is localized between the interfaces  $y_{j-1}$  and  $y_j$ .

Fig. 5 represents calculations at 0 degree angle and wavelength 550 nm for squared electric fields (total,  $s$ -polarization and  $p$ -polarization), photon flux density (total, forward and backward flux) and

absorption rate (total,  $s$ -polarization and  $p$ -polarization). Fig. 6 graphs the same as Fig. 5 but at 80 degrees angle. These figures show that the optical absorption is mainly localized in the photoelectrode with a very high absorption rate at the beginning of the photoelectrode and platinum layer (the latter is not clearly appreciated in the figure due to the thinness of the Pt film). Additionally, the backward flux density is practically zero compared with the forward flux density from the incoming medium due to the strong absorption by the photoelectrode at this wavelength (550 nm, See Figure 4). As expected, at 80 degrees angle (Fig. 6) there is a clear difference between the two polarizations whereas at zero angle there is no difference (Fig. 5). The total absorption at 80 degrees angle is mainly localized in the photoelectrode, and comes more pronouncedly from the  $p$ -polarization wave than from the  $s$ -polarization. These energetic calculations show the power of the exact solution when SBM and Pointing Theorem are applied.

Hence, the objective of this study has been achieved using a general symmetry theory that explains and avoids numerical instabilities, which has been illustrated via computer calculations. The geometrical interpretation of the numerical solution yields a clear insight into its geometric-physical properties. We argue that this model can generally be used for applications in many fields of science and technology that require a fast solution without instabilities by using a simple method.

## 5. Conclusions

In this paper, we developed a symmetry-based method (SBM) and specifically applied it to obtain the equivalent solutions of the Maxwell's equations in the TMM representation and in a parameterized form. We have tailored the parameter to obtain an exact solution, that is, a solution where TMM does not contain numerical instabilities. This exact solution could be applied for region-by-region calculations done in interactive systems with a constant refractive index (region-by-region homogeneous and isotropic structures) or refractive index that varies in a point-wise manner (inhomogeneous and isotropic structures). At any rate, the  $m$ - parameter TMM solution does not increase the computer time with respect to the  $0$ - parameter TMM solution. That is because all of the time consumption practically comes from

matrix multiplications that are invariant, since the SBM preserves the TMM matrix structure, and because the external symmetries of the TMM have a scalar structure that contributes only on a negligibly to the total computer time. The SBM demonstrates that it is possible to obtain new solutions via transformations in its reference systems, which corresponds to mapping its associated solutions. The SBM is solely based on the symmetries of the TMM structure; therefore, it can be applied not only to resolve Maxwell's equations but also to resolve any kind of classical or quantum one-, two-, or three-dimensional linear system that involves wave propagation. The advantages of the exact solution are based on its easy implementation, computer time efficiency, stability and physical meaning, which in our opinion justify the effort taken to understand the mathematical structure of the TMM in detail.

### **Acknowledgements**

This work was partially funded by the Nordic Innovation Center project, NORDIC DSC (no. 09053) and the CNB-E project of the TKK/Aalto University Multidisciplinary Institute of Digitalisation and Energy (MIDE).

## References

- [1] J. D. Joannopoulos, *Photonic Crystals, Molding the Flow of Light*. Princeton: Princeton University Press, 2008
- [2] A. Jiménez-Solano, C. López-López, O. Sánchez-Sobrado, J. M. Luque-Raigon, M. E. Calvo, C. Fernández-López, Ana Sánchez-Iglesias, L. M. Liz-Marzán, and H. Míguez, Integration of Gold Nanoparticles in Optical Resonators, *Langmuir* **28** (24), 9161–9167 (2012)
- [3] A. J. Ward and J. B. Pendry, Refraction and geometry in Maxwell's equations, *J. Mod. Optic.* **43**, 773-793 (1996)
- [4] P. Yeh, *Optical Waves in Layered Media*. Hoboken: Wiley-Interscience, 2005, chap. 6
- [5] M. G. Moharam, D. A. Pommet, E. B. Grann and T. K. Gaylord, Stable implementation of the rigorous coupled-wave analysis for surface-relief gratings: enhanced transmittance matrix approach, *J. Opt. Soc. Am. A* **12**,1077-1086 (1995)
- [6] D. Y. K. Ko and J. R. Sambles, Scattering Matrix Method for propagation of radiation in stratified media: attenuated total reflection studies of liquid crystals, *J. Opt. Soc. Am. A* **5**,1863-1866 (1988)
- [7] S. G. Johnson and J. D. Joannopoulos, Block-iterative frequency-domain methods for Maxwell's equations in a planewave basis, *Opt. Express* **8** (3), 173–190 (2000)
- [8] K. Busch, G. von Freymann, S. Linden, S.F. Mingaleev, L. Tkeshelashvili and M. Wegener, Periodic nanostructures for photonics, *Phys. Rep.* **444**, 101–202 (2007)
- [9] Z. Y. Li and L. L. Lin, Photonic band structures solved by a plane-wave-based transfer-matrix method, *Phys. Rev. E* **67**, 046607 (2003)
- [10] D. J. Cha, J. H. Kim and Y. J. Joo, Analysis of the combustion instability of a model gas turbine combustor by the transfer matrix method, *J. Mech. Sci. Tech.* **23**, 1602 – 1612 (2009)
- [11] H. Yin and R. Tao, Improved transfer matrix method without numerical instability, *EPL* **84**, 57006 (2008)

- [12] M. Suzuki, Transfer-matrix method and Monte Carlo simulation in quantum spin systems, *Phys. Rev. B* **31**, 2957 – 2965 (1985)
- [13] S. Wenger, M. Schmid, G. Rothenberger, A. Gentsch, M. Grätzel and J. O. Schumacher, Coupled optical and electronic modeling of dye-sensitized solar cells for steady-state parameter extraction, *J. Phys. Chem. C* **115**, 10218-10229 (2011)
- [14] D. W. Lynch and W. R. Hunter, *Comments on the Optical Constants of Metals and an Introduction to the Data for Several Metals*, in *Handbook of Optical Constants of Solids*, E. D. Palik (ed.), San Diego: Academic Press, 1998, Vol. I, pp. 333-341 and Vol III, pp. 240-249

## Figure Captions

**Figure 1.** Structure of the dye-sensitized solar cell (DSSC) with the different layers marked with subscript  $j=1,\dots,6$ . The complex refractive indices for layers are graphed in figure 3. The electromagnetic field propagation is given for a generic  $j$ -layer of the structure showing the  $s$ -polarization and  $p$ -polarization for the forward wave only. The backward wave is omitted by simplicity. The origin position is  $y_0 = 0$ .

**Figure 2.** Comparison between the calculations with the exact solution and the experimental data from reference [13] for a) reflectance, b) transmittance and c) absorptance of a dye-sensitized solar cell (DSSC) with a  $8.3 \mu\text{m}$  thick  $\text{TiO}_2$  film dyed with Z907 as a photoelectrode. The DSSC parameters are taken from reference [13]. The accuracy between the calculated exact solution (simu l) and the calculated (simu w) and experimental (data) from reference [13] is inside 4%.

**Figure 3.** a) Real refractive indices used in the metallic-dielectric multilayer. b) Imaginary refractive indices used in the metallic-dielectric multilayer and c) detailed illustration of low scale refractive indices. The refractive indices of metals were taken from [14] and the dielectrics from [13].

**Figure 4.** Calculations with exact solution at angles a) 0, b) 40 and c) 80 for the total reflectance, absorptance by different layer, and total transmittance with the refractive indices given in figure 3 (see text). At each wavelength the light is distributed between transmitted (1.), absorbed by different layers (2.-7.) and reflected (8.) light in the DSSC. The transmittance is practically zero in the entire wavelength range.

**Figure 5.** Optical calculations represented at angle 0 and wavelength 550 nm for a) squared electric fields, b) photon flux density and c) absorption rate. The *s*- and *p*-polarizations are overlapping in figures a and c. The total and the forward flux are overlapping in figure b.

**Figure 6.** Optical calculations represented at angle 80 and wavelength 550 nm for a) squared electric fields, b) photon flux density and c) absorption rate. The total and the forward flux are overlapping in figure part b.

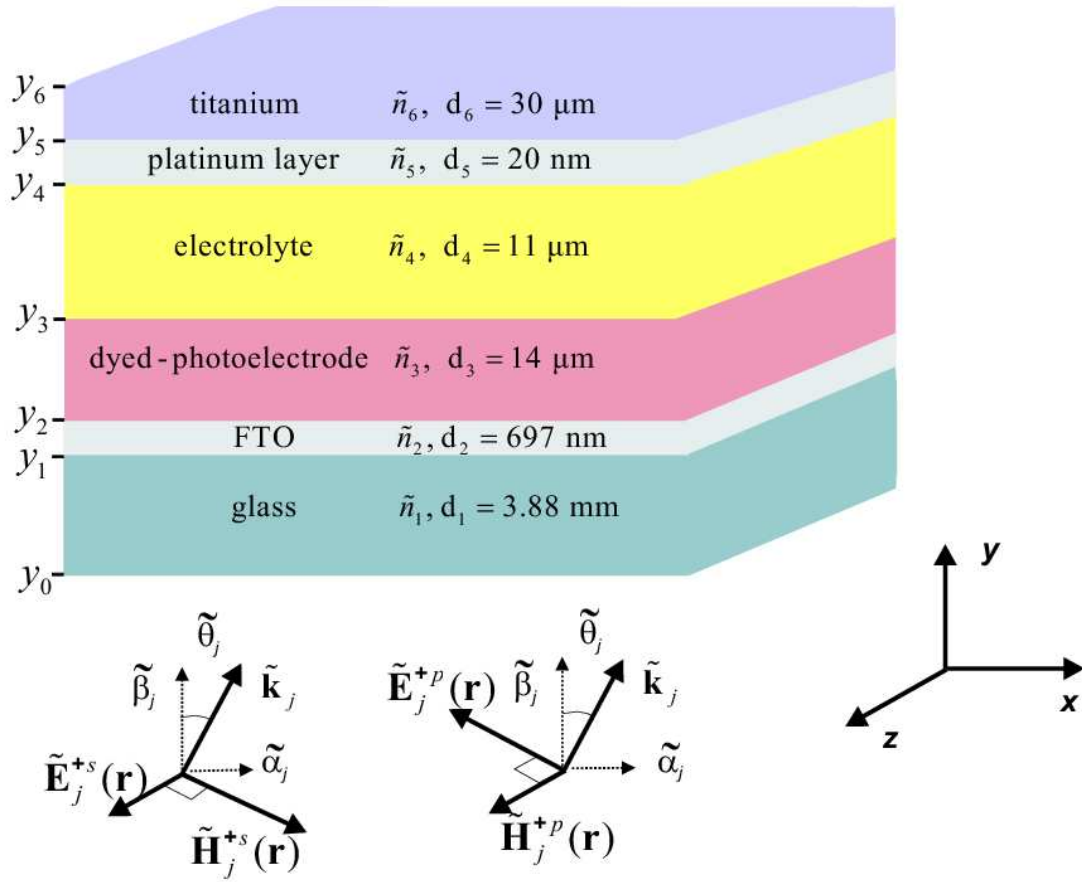


**Figure 1.** Structure of the dye-sensitized solar cell (DSSC) with the different layers marked with subscript  $j=1,\dots,6$ . The complex refractive indices for layers are graphed in figure 3. The electromagnetic field propagation is given for a generic  $j$ -layer of the structure showing the  $s$ -polarization and  $p$ -polarization for the forward wave only. The backward wave is omitted by simplicity. The origin position is  $y_0 = 0$ .



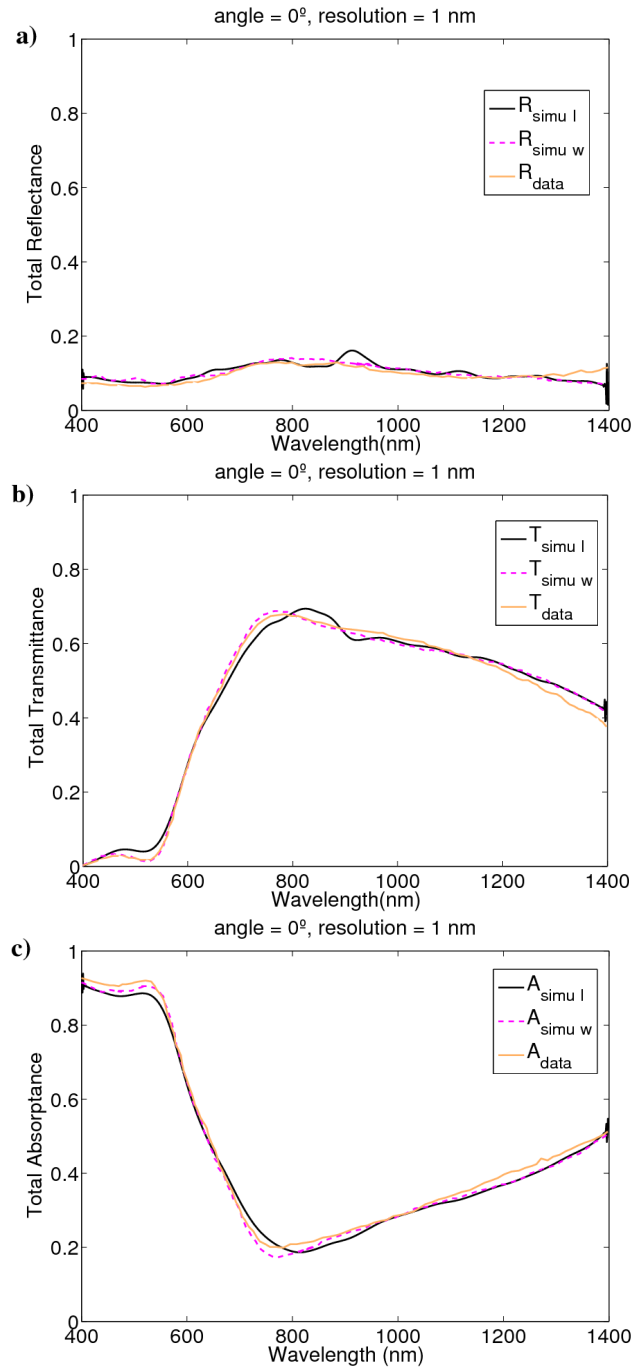


**Figure 2.** Comparison between the calculations with the exact solution and the experimental data from reference [13] for a) reflectance, b) transmittance and c) absorbance of a dye-sensitized solar cell (DSSC) with a 8.3  $\mu\text{m}$  thick  $\text{TiO}_2$  film dyed with Z907 as a photoelectrode. The DSSC parameters are taken from reference [13]. The accuracy between the calculated exact solution (simu l) and the calculated (simu w) and experimental (data) from reference [13] is inside 4%.

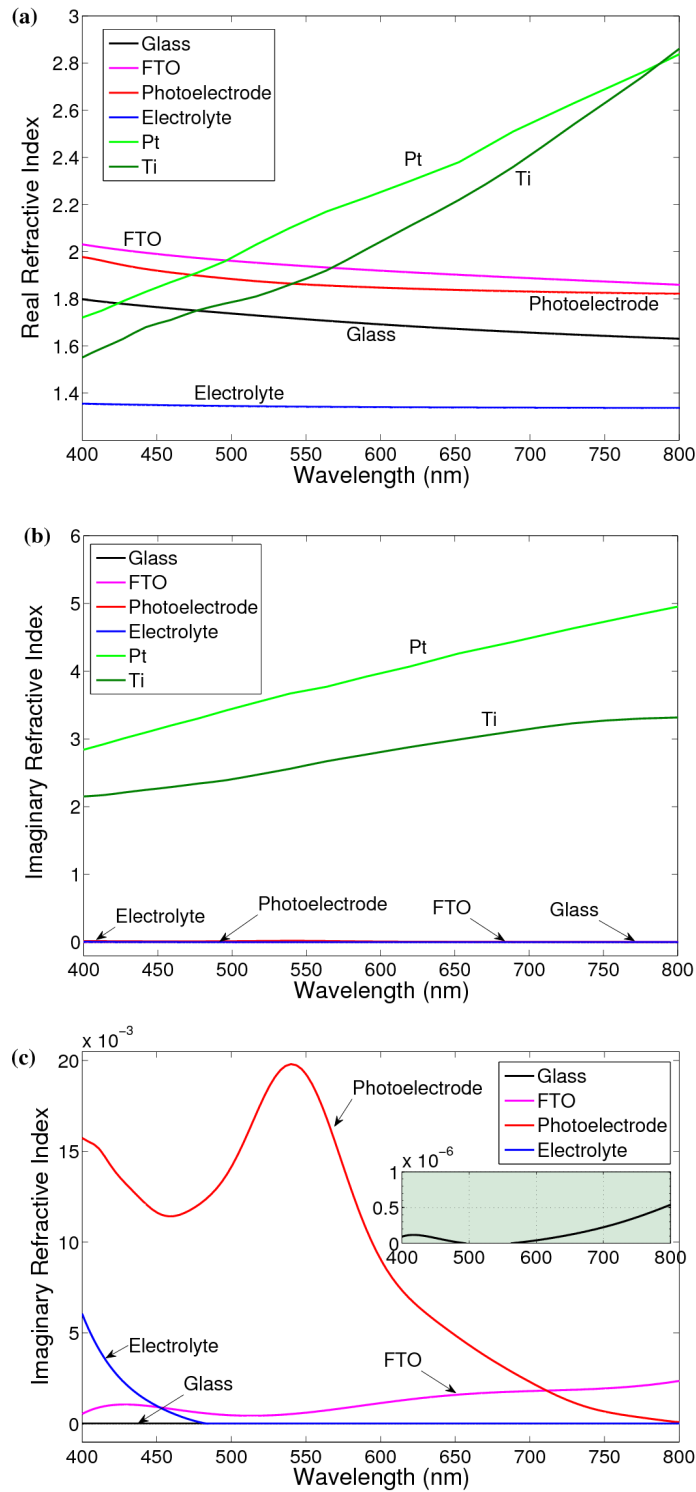


**Figure 3.** a) Real refractive indices used in the metallic-dielectric multilayer. b) Imaginary refractive indices used in the metallic-dielectric multilayer and c) detailed illustration of low scale refractive indices. The refractive indices of metals were taken from [14] and the dielectrics from [13].

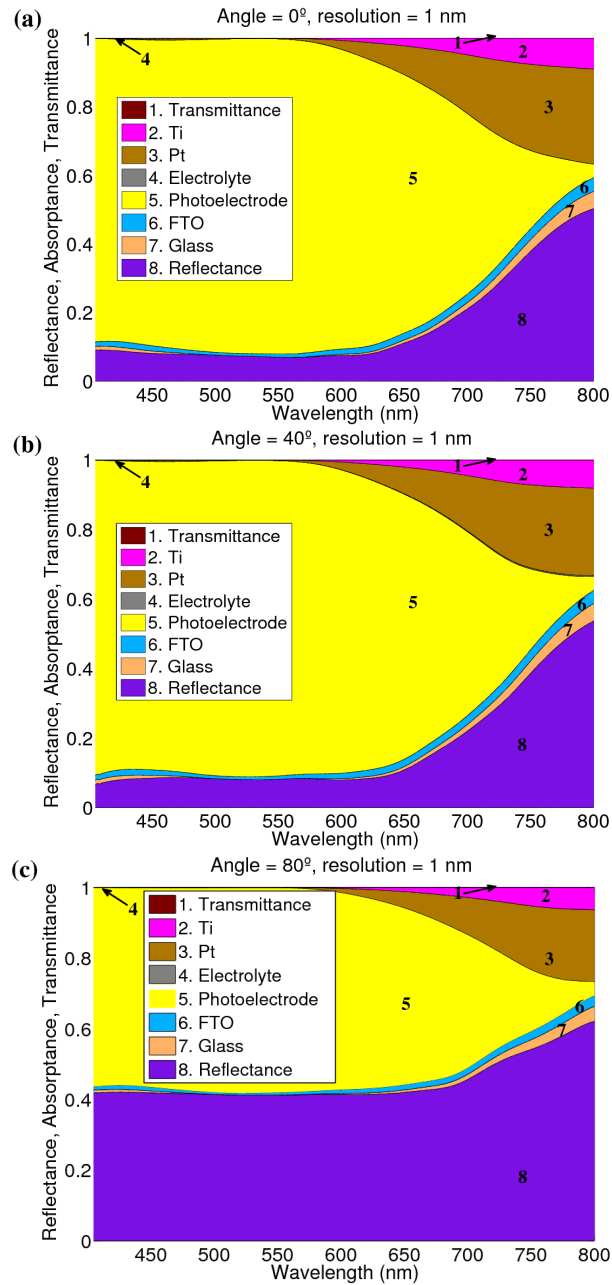


**Figure 4.** Calculations with exact solution at angles a) 0, b) 40 and c) 80 for the total reflectance, absorbance by different layer, and total transmittance with the refractive indices given in figure 3 (see text). At each wavelength the light is distributed between transmitted (1.), absorbed by different layers (2.-7.) and reflected (8.) light in the DSSC. The transmittance is practically zero in the entire wavelength range.

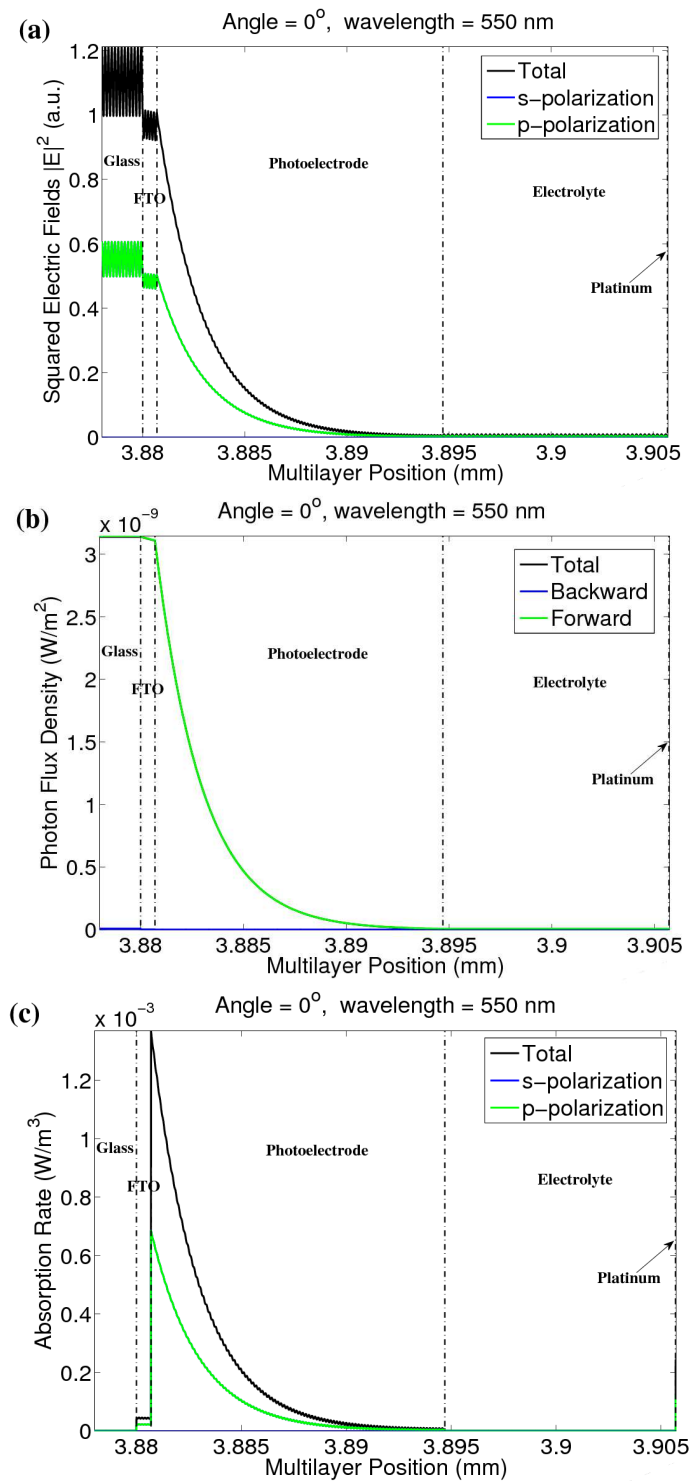


**Figure 5.** Optical calculations represented at angle 0 and wavelength 550 nm for a) squared electric fields, b) photon flux density and c) absorption rate. The *s*- and *p*-polarizations are overlapping in figures a and c. The total and the forward flux are overlapping in figure b.

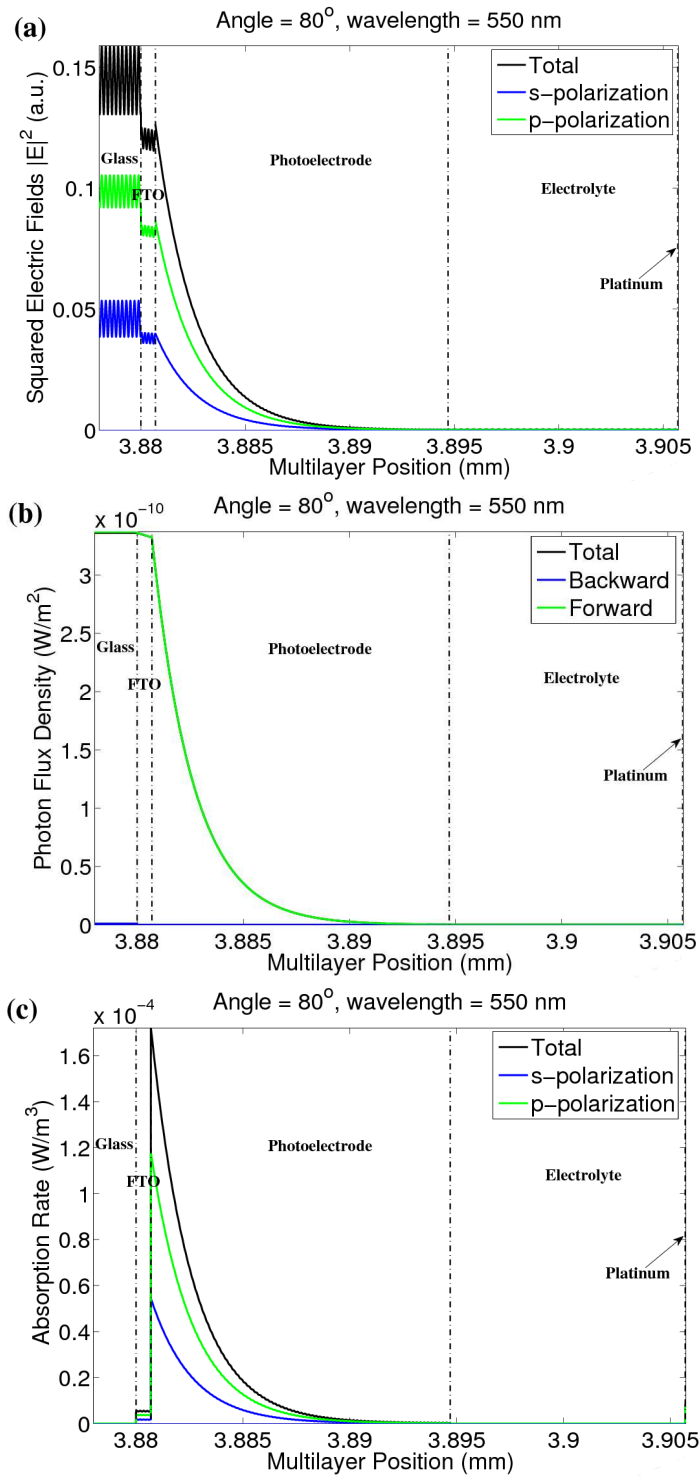


**Figure 6.** Optical calculations represented at angle 80 and wavelength 550 nm for a) squared electric fields, b) photon flux density and c) absorption rate. The total and the forward flux are overlapping in figure part b.